Alternative Solvers for the Derivative Riemann Problem for Hyperbolic Balance Laws

C. E. Castro and E. F. Toro
Laboratory of Applied Mathematics, Faculty of Engineering
University of Trento, Trento, Italy
e-mail: castroc@ing.unitn.it, toro@ing.unitn.it

Abstract

We study methods for solving the Cauchy problem for systems of non-linear hyperbolic balance laws with initial condition consisting of two smooth vectors, with a discontinuity at the origin. We call this initial-value problem the Derivative Riemann Problem, or DRP. Two new methods of solution are presented. The first one results from a re-interpretation of the high-order numerical methods proposed by Harten et al. [10] and the second method is a modification of the DRP solver in [35]. A systematic assessment of all available DRP solvers is carried out and their relative merits are discussed. Finally, we also implement the DRP solvers, locally, in the context of high-order finite volume numerical methods of the ADER type, on unstructured meshes. Schemes of up to fifth order of accuracy in space and time for the two-dimensional compressible Euler equations are constructed. Empirically obtained convergence rates are studied systematically and, for the tests considered, these correspond to the theoretically expected orders of accuracy.

1 Introduction

The *classical Riemann problem* is the Cauchy problem for a system of conservation laws, with initial condition consisting of two *constant* states separated by a discontinuity. The solution of this Riemann problem was first used by Godunov to construct his first-order upwind numerical scheme [9]. Methods to solve the classical Riemann problem are studied, for example, in [32]. The so-called *generalized Riemann problem*, in which the initial condition consists of two polynomials of first degree (vectors) separated by a discontinuity at the interface, has been used to construct Godunov-type schemes of second order of accuracy [20], [37], [1], [4], [3], [19], [30], [31], [32], [2].

The more general Cauchy problem with initial conditions consisting of two smooth functions separated by a discontinuity at the origin has also been studied in recent years; this is the theme of this paper. We call this Cauchy problem the *Derivative Riemann Problem*, or DRP, to distinguish it from the terminology *Generalized Riemann problem*, mostly associated with the simpler problem with piece-wise linear initial conditions. Theoretical aspects regarding the DRP are found in [17], [18] and references therein.

A method to solve the Derivative Riemann Problem was presented in [35], which is a generalization to arbitrary order of the MGRP approach communicated in [30], [31] for second-order schemes, to solve non-linear hyperbolic systems. The method of [35] is applicable to non-linear hyperbolic systems with source terms. The technique expresses the time-dependent solution at the interface as a power series expansion of order K. The leading term of the expansion is the solution of a classical, usually non-linear, Riemann problem. The determination of the higher order terms involves the Cauchy-Kowalewski method to express time derivatives in terms of functions whose arguments are spatial derivatives. In order to define the spatial derivatives one first constructs new evolution equations for these and then solves additional classical Riemann problems. The solutions of these classical Riemann problems define all spatial derivatives at the interface. The complete solution is then built up by evaluating the functions of spatial

derivatives and assembling the complete series. In this manner the method of solution of order K boils down to solving 1 classical non-linear Riemann problem for the leading term and K classical linear Riemann problems for spatial derivatives. An extended version of the method to deal with more general hyperbolic systems is presented in [33].

Numerical methods of arbitrary order of accuracy can be constructed as a straight generalization of Godunov's first order method, by using the solution of the DRP at the interface. This methods were called ADER methods in [34], where schemes of arbitrary accuracy were formulated for linear problems in one and multiple space dimensions. Corresponding schemes for non-linear systems based on the DRP solver in [35], were reported in [28], [36] and [29]. Further developments of ADER schemes are reported in [27], [23], [24], [22], [14], [15], [16], [7], [5].

The present paper is motivated by number of issues. First, it appears necessary to examine more closely the quality of the approximate solutions produced by the existing DRP solver of Toro and Titarev [35], for the case of non-linear systems. In addition, we have recently identified a class of problems for which this DRP solver may experience some difficulties. The problems in question include, locally, a stationary discontinuity, a shock wave or a contact wave, for which the DRP expansion of [35] may be non-unique, giving rise to a non-unique choice of intercell numerical flux. At the level of the first-order scheme the choice is unique due to the Rankine-Hugoniot conditions that ensure the continuity of the flux; that is, the flux is the same whether it is taken from the left or from the right of the interface. For the high-order schemes the fluxes are different. We also present new DRP solvers and discuss their relative performance, at the local level, as well as a means to provide a numerical flux for high-order methods. The high-order method first proposed by Harten, Engquist, Osher and Chakravarthy [10], after a minor modification, may be interpreted in the frame of the ADER methods. That is, we could define an associated derivative Riemann problem with a corresponding method to solve it. We call the resulting method the HEOC solver. We also propose a new solver that is a modification of the Toro-Titarev solver. The main feature of this DRP solver is that the high-order terms are computed by solving linearized classical Riemann problems for the high-order *time derivatives*. This is motivated by the fact that for a linear system, all-order time derivatives obey the original system of PDEs. We note that for the case of a linear system with constant coefficients all three methods studied here coincide and their solution is identical to the exact solution of the DRP problem.

A systematic assessment of the methods to solve the DRP for non-linear systems is performed, through a carefully selected suite of test problems. We also implement some of the schemes to construct high order numerical methods to solve the general initial boundary value problem. The methods are implemented and assessed for one dimensional problems and for two-dimensional problems on unstructured meshes.

The rest of this paper is organized as follows. In Sect. 2 we define the mathematical problem and review an existing DRP solver. In Sect. 3 we present new DRP solvers. Sect. 4 deals with the DRP solvers in the context of high-order finite volume methods in one-space dimension. In Sect. 5 we assess the performance of the local DRP solvers. In Sect. 6 we construct ADER high order numerical methods for two-dimensional systems on unstructured meshes. Conclusions are drawn in Sect. 7.

2 The Derivative Riemann Problem

Here we first state the mathematical problem and then briefly review an existing semi-analytical method to compute the solution at the interface as a function of time.

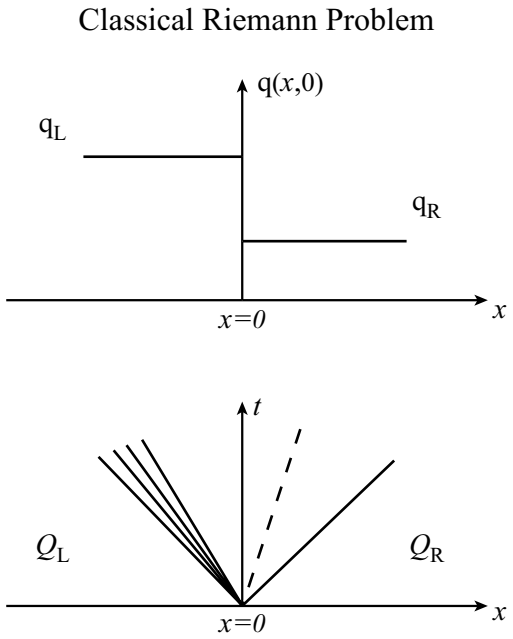

Figure 1: The classical Riemann problem for a typical 3×3 non-linear system. Top frame: initial condition at $t = 0$ for a single component q of the vector of unknowns $\mathbf{Q}$. Bottom frame: structure of the solution on the $x - t$ plane.

2.1 The Mathematical Problem

The Derivative Riemann Problem is the initial-value problem

$$\left.\begin{array}{lll} \text{PDEs:} & \partial_t \mathbf{Q} + \partial_x \mathbf{F}(\mathbf{Q}) = \mathbf{S}(\mathbf{Q}) \ , \quad x \in (-\infty, \infty) \ , \quad t > 0 \ , \\ \text{IC:} & \mathbf{Q}(x,0) = \left\{ \begin{array}{ll} \mathbf{Q}_L(x) & \text{if} \quad x < 0 \ , \\ \mathbf{Q}_R(x) & \text{if} \quad x > 0 \ . \end{array} \right. \end{array} \right\} \tag{1}$$

The partial differential equations (PDEs), with source terms, are assumed to be a general system of hyperbolic balance laws. The initial condition (IC) consists of two vectors $\mathbf{Q}_L(x)$, $\mathbf{Q}_R(x)$, the components of which are assumed to be smooth functions of x, with K continuous non-trivial spatial derivatives away from zero. We denote by DRP_K the Cauchy problem (1). In the DRP_0 all first and higher-order spatial derivatives of the initial condition away from the origin vanish identically; this case corresponds to the *classical* piece-wise constant data Riemann problem, associated with the first-order Godunov scheme [9]. Similarly, in the DRP_1 all second and higher-order spatial derivatives of the initial condition for the DRP away from the origin vanish identically; this case corresponds to the piece-wise linear data Riemann problem, or the so-called generalized Riemann problem (GRP), associated with a second-order method of the Godunov type [20], [37], [1], [4], [3], [19], [31], [2].

Fig. 1 depicts the classical Riemann problem DRP_0 for a typical 3×3 non-linear system for which it is assumed that the left wave is a rarefaction, the right wave is a shock and the middle wave is a contact. The top frame shows the initial condition for a single component q of the vector of unknowns $\mathbf{Q}$. The bottom frame of Fig. 1 depicts the structure of the corresponding solution on the $x - t$ plane; characteristics curves are straight lines. Fig. 2 illustrates the Derivative Riemann Problem DRP_K; the top frame depicts the initial condition for a single

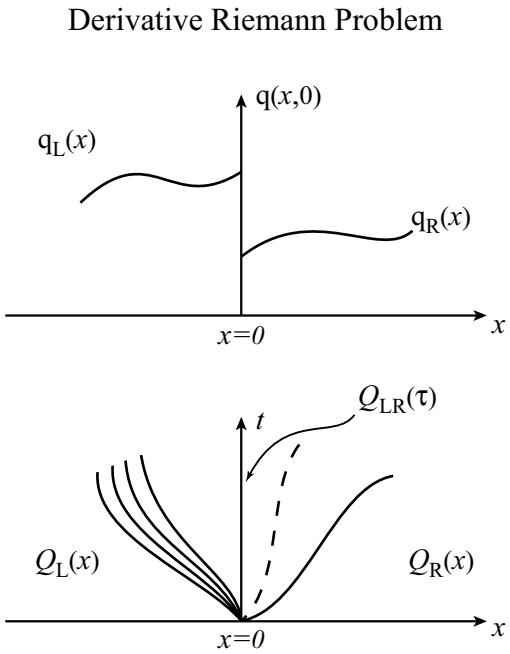

Figure 2: The Derivative Riemann Problem for a typical 3×3 non-linear system. Top frame: initial condition at $t = 0$ for a single component q of the vector of unknowns $\mathbf{Q}$. Bottom frame: structure of the solution on the $x - t$ plane.

component q and consists of two smooth functions separated by a discontinuity at the origin. The bottom frame of Fig. 2 depicts the corresponding structure of the solution on the $x - t$ plane. Now characteristics are no longer straight lines. Compare Figs. 1 and 2. The aim of this paper is to present methods to find the solution of (1) at the origin $x = 0$ and for $t > 0$, as a function of time and represented by $Q_{LR}(\tau)$ in Fig. 2. Recall that for the classical Riemann problem the solution is self-similar, it depends on the ratio x/t and is constant at $x = 0$ (the interface) for $t > 0$. In many situations of interest one can find the solution everywhere in the half plane $x \in (-\infty, \infty)$, $t > 0$, although for the purpose of computing a numerical flux, knowing the solution along the interface is sufficient. For the derivative Riemann problem DRP_K, with $K > 0$, finding the solution in the half plane $x \in (-\infty, \infty)$, $t > 0$, is a formidable task that is possible only in special cases. See [19] for the complete solution of the DRP_1 for the Euler equations for ideal gases.

To construct high-order numerical methods of the ADER type [34] it is sufficient to find the solution $\mathbf{Q}_{LR}(\tau)$ at the interface position $x = 0$, as a function of time τ alone. $\mathbf{Q}_{LR}(\tau)$ will provide sufficient information to compute a numerical flux to construct a numerical scheme of $(K + 1)$-th order of accuracy in both space and time. The corresponding intercell numerical flux, denoted by $\mathbf{F}_{LR}$, is the time-integral average

$$\mathbf{F}_{LR} = \frac{1}{\Delta t} \int_0^{\Delta t} \mathbf{F}(\mathbf{Q}_{LR}(\tau)) d\tau \ , \tag{2}$$

where Δt is the time step of the scheme. Numerical methods based on this framework were called ADER methods in [34]. Early versions of the approach were communicated in [30], [31].

Note that the conventional case of piece-wise constant data reproduces the classical first-order upwind method of Godunov [9].

2.2 A Known Method of Solution

Here we briefly review the method proposed by Toro and Titarev [35], [33], whereby a semi-analytical solution of the Derivative Riemann Problem (1) is obtained. Their method, as in [1] for second order and in [17] for the general case, first expresses the sought solution $\mathbf{Q}_{LR}(\tau)$ at the interface $x = 0$ as the power series expansion in time

$$\mathbf{Q}_{LR}(\tau) = \mathbf{Q}(0, 0_+) + \sum_{k=1}^{K} \left[\partial_t^{(k)} \mathbf{Q}(0, 0_+)\right] \frac{\tau^k}{k!} , \tag{3}$$

where

$$\mathbf{Q}(0, 0_+) = \lim_{t \to 0_+} \mathbf{Q}(0, t) .$$

The solution contains the leading term $\mathbf{Q}(0, 0_+)$ and higher-order terms, with coefficients determined by the time derivatives $\partial_t^{(k)} \mathbf{Q}(0, 0_+)$. The determination of all terms in the expansion includes the following steps:

Step (I): The leading term. To compute the leading term one solves exactly or approximately the conventional Riemann problem

$$\left.\begin{array}{lll} \text{PDEs:} & \partial_t \mathbf{Q} + \partial_x \mathbf{F}(\mathbf{Q}) = \mathbf{0} , & \\ \text{ICs:} & \mathbf{Q}(x, 0) = \left\{ \begin{array}{lll} \mathbf{Q}_L(0_-) & \text{if} & x < 0 , \\ \mathbf{Q}_R(0_+) & \text{if} & x > 0 , \end{array} \right. & \end{array}\right\} \tag{4}$$

with

$$\mathbf{Q}_L(0_-) = \lim_{x \to 0_-} \mathbf{Q}_L(x) , \quad \mathbf{Q}_R(0_+) = \lim_{x \to 0_+} \mathbf{Q}_R(x) . \tag{5}$$

The similarity solution of (4) is denoted by $\mathbf{D}^{(0)}(x/t)$ and the leading term in (3) is

$$\mathbf{Q}(0, 0_+) = \mathbf{D}^{(0)}(0) . \tag{6}$$

Step (II): Higher order terms. There are three sub-steps here.

1. **Time derivatives in terms of spatial derivatives:** Use the Cauchy-Kowalewski method to express time derivatives in (3) in terms of functions of space derivatives

$$\partial_t^{(k)} \mathbf{Q}(x, t) = \mathbf{G}^{(k)}(\partial_x^{(0)} \mathbf{Q}, \partial_x^{(1)} \mathbf{Q}, \ldots, \partial_x^{(k)} \mathbf{Q}) . \tag{7}$$

   The source terms $\mathbf{S}(\mathbf{Q})$ in (1) are all included in the arguments of the functions $\mathbf{G}^{(k)}$. The problem now is that of determining the arguments of $\mathbf{G}^{(k)}$, namely the spatial derivatives at the interface.

2. **Evolution equations for derivatives:** Construct evolution equations for spatial derivatives

$$\partial_t(\partial_x^{(k)} \mathbf{Q}(x, t)) + \mathbf{A}(\mathbf{Q}) \partial_x(\partial_x^{(k)} \mathbf{Q}(x, t)) = \mathbf{H}^{(k)} , \tag{8}$$

   where $\mathbf{A}(\mathbf{Q})$ is the Jacobian matrix of the PDEs in (1).

3. **Riemann problems for spatial derivatives:** Simplify (8) by neglecting the right-hand side terms $\mathbf{H}^{(k)}$ and linearizing the evolution equations. Then pose classical, homogeneous linearized Riemann problems for spatial derivatives

$$\left.\begin{array}{ll} \text{PDEs:} & \partial_t(\partial_x^{(k)}\mathbf{Q}(x,t)) + \mathbf{A}_{LR}^{(0)}\partial_x(\partial_x^{(k)}\mathbf{Q}(x,t)) = \mathbf{0}\ , \\ \text{ICs:} & \partial_x^{(k)}\mathbf{Q}(x,0) = \begin{cases} \partial_x^{(k)}\mathbf{Q}_L(0_-) & \text{if} \quad x<0\ , \\ \partial_x^{(k)}\mathbf{Q}_R(0_+) & \text{if} \quad x>0\ , \end{cases} \end{array}\right\} \tag{9}$$

with $\mathbf{A}_{LR}^{(0)} = \mathbf{A}(\mathbf{Q}(0,0_+))$. Solve these Riemann problems to obtain similarity solutions $\mathbf{D}^{(k)}(x/t)$ and set

$$\partial_x^{(k)}\mathbf{Q}(0,0_+) = \mathbf{D}^{(k)}(0)\ . \tag{10}$$

Step (III): The solution. Form the solution as the power series expansion:

$$\mathbf{Q}_{LR}(\tau) = \mathbf{C_0} + \mathbf{C_1}\tau + \mathbf{C_2}\tau^2 + \ldots + \mathbf{C_K}\tau^K\ , \tag{11}$$

with $\mathbf{C}_0$ as in (6) and

$$\mathbf{C}_k \equiv \frac{\partial_t^{(k)}\mathbf{Q}(0,0_+)}{k!} = \frac{\mathbf{G}^{(k)}(\mathbf{D}^{(0)}(0),\mathbf{D}^{(1)}(0),\ldots,\mathbf{D}^{(k)}(0))}{k!}\ , \tag{12}$$

for $k = 1,\ldots,K$.

This solution technique for the Derivative Riemann Problem DRP_K reduces the problem to that of solving $K+1$ classical homogeneous Riemann problems, one (generally non-linear) Riemann problem to compute the leading term and K linearized Riemann problems to determine the higher order terms.

The leading term requires the availability of a *Riemann solver*, exact or approximate. The K linearized Riemann problems (9) for most well-known systems associated with the higher order terms can be solved analytically and no choice of a *Riemann solver* is necessary. Moreover, all of these linearized problems have the same eigenstructure, as the coefficient matrix is the same for all Riemann problems for derivatives.

In principle, the technique can be applied to calculate the early-time solution of advection-reaction equations with piece-wise smooth initial conditions. One can set up a derivative Riemann problem at any desired position, taking care that at each point $x = x_d$ of discontinuity in the initial condition one sets a corresponding derivative Riemann problem centred at x_d. The solution at each point x_d, for a small time τ, can be used to check the results of numerical schemes.

3 Other Methods of Solution

Here we study two alternative methods for solving the DRP (1). The first results from a re-interpretation of the high-order numerical method first proposed by Harten, Engquist, Osher and Chakravarthy [10]. Consequently we call this derivative Riemann solver, the HEOC solver. The second method we study results from a modification of both the Toro-Titarev solver [35] of section 2.2 and the HEOC solver. We denote this method of solution as the CT solver.

3.1 Interaction of Power-Series Expansions

Here we re-interpret the method proposed by Harten, Engquist, Osher and Chakravarthy [10] to compute numerical fluxes for their high-order methods, as a technique to provide an approximate solution to the derivative Riemann problem (1) at the interface $x = 0$, as a function of time. They proposed power series expansions in space and time for the solution in each control volume, or cell. There followed the application of the Cauchy-Kowalewski method to convert all time derivatives in the expansions to space derivatives, which in turn could be computed on the initial data.

In our re-interpretation we include source terms in the equations and consider power series expansions in time on each side of the interface

$$\tilde{\mathbf{Q}}_L(\tau) = \mathbf{Q}_L(0_-) + \sum_{k=1}^{K} \left[\partial_t^{(k)} \mathbf{Q}(0_-, 0)\right] \frac{\tau^k}{k!} \tag{13}$$

and

$$\tilde{\mathbf{Q}}_R(\tau) = \mathbf{Q}_R(0_+) + \sum_{k=1}^{K} \left[\partial_t^{(k)} \mathbf{Q}(0_+, 0)\right] \frac{\tau^k}{k!} \ , \tag{14}$$

with

$$\mathbf{Q}(0_-, 0) = \lim_{x \to 0_-} \mathbf{Q}(x, 0) \equiv \mathbf{Q}_L(0_-) \tag{15}$$

and

$$\mathbf{Q}(0_+, 0) = \lim_{x \to 0_+} \mathbf{Q}(x, 0) \equiv \mathbf{Q}_L(0_+) \ . \tag{16}$$

The Cauchy-Kowalewski method allows us to use the PDEs in (1) to express all time derivatives in (13), (14) as functions of space derivatives and of the source terms $\mathbf{S}(\mathbf{Q})$, namely

$$\partial_t^{(k)} \mathbf{Q}(x, t) = \mathbf{G}^{(k)}(\partial_x^{(0)} \mathbf{Q}, \partial_x^{(1)} \mathbf{Q}, \ldots, \partial_x^{(k)} \mathbf{Q}) \ . \tag{17}$$

These expressions are well defined to the left and right of the interface, given that the initial conditions in (1) are assumed to be smooth away from 0. We can also define the limiting values from left and right, at $t = 0$, of the spatial derivatives of the initial conditions

$$\mathbf{Q}_L^{(k)}(0_-) \equiv \lim_{x \to 0_-} \frac{d^k}{dx^k} \mathbf{Q}_L(x) \ , \tag{18}$$

$$\mathbf{Q}_R^{(k)}(0_+) \equiv \lim_{x \to 0_+} \frac{d^k}{dx^k} \mathbf{Q}_R(x) \ . \tag{19}$$

Thus we have

$$\partial_t^{(k)} \mathbf{Q}(0_-, 0) = \mathbf{G}^{(k)}(\mathbf{Q}_L^{(0)}(0_-), \mathbf{Q}_L^{(1)}(0_-), \ldots, \mathbf{Q}_L^{(k)}(0_-)) \ , \tag{20}$$

and

$$\partial_t^{(k)} \mathbf{Q}(0_+, 0) = \mathbf{G}^{(k)}(\mathbf{Q}_R^{(0)}(0_+), \mathbf{Q}_R^{(1)}(0_+), \ldots, \mathbf{Q}_R^{(k)}(0_+)) \ . \tag{21}$$

We define the solution of the DRP (1) at the interface $x = 0$, at time $t = \tau$ as

$$\mathbf{Q}_{LR}(\tau) = \mathbf{D}(\tau, 0) \ , \tag{22}$$

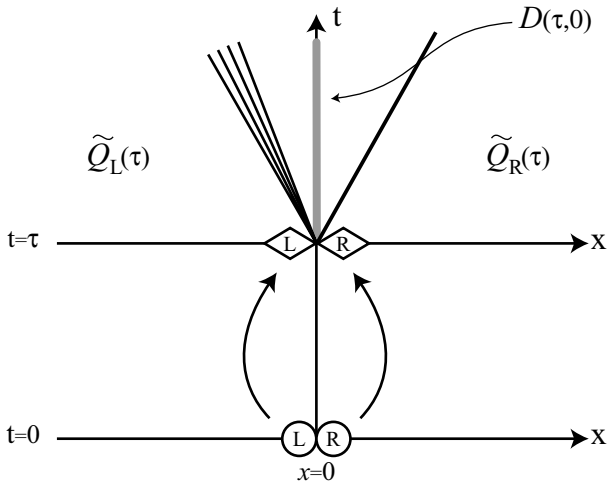

Figure 3: Illustration of the HEOC Derivative Riemann Problem solver. The limiting values of the initial data from left and right (circles) are time evolved separately to any time τ (rhombuses). The desired solution results from solving the classical Riemann problem with these evolved states as data.

where now $\mathbf{D}(\tau, x/(t-\tau))$ is the similarity solution of the classical, homogeneous Riemann problem

$$\left.\begin{array}{lll} \text{PDEs:} & \partial_t \mathbf{Q} + \partial_x \mathbf{F}(\mathbf{Q}) = \mathbf{0}\,, & \\ \text{ICs:} & \mathbf{Q}(x,0) = \left\{ \begin{array}{lll} \tilde{\mathbf{Q}}_L(\tau) & \text{if} & x < 0\,, \\ \tilde{\mathbf{Q}}_R(\tau) & \text{if} & x > 0\,. \end{array} \right. & \end{array}\right\} \tag{23}$$

Note that here $\mathbf{D}(\tau, x/(t-\tau))$ depends on the parameter τ. We call this re-interpretation of the method proposed by Harten et al. [10] as a derivative Riemann solver, the HEOC solver.

Fig. 3 gives an interpretation of the HEOC solution method for the DRP (1). At time $t = 0$ one performs a Taylor series expansion in time on the limiting values of the data left and right of the interface (circles). Upon the application of the Cauchy-Kowalewski method one evolves the data in time on each side of the interface to yield time-evolved states $\tilde{\mathbf{Q}}_L(\tau)$ and $\tilde{\mathbf{Q}}_R(\tau)$, at any chosen time $t = \tau$ (rhombuses in Fig. 3). These (constant) states at $t = \tau$ form the initial conditions for a classical Riemann problem, as depicted on the top part of Fig. 3 by the self-similar wave pattern. The sought solution is that given by (22), which is constant along the t-axis associated with the self-similar wave pattern. As the method applies to any time τ one has a time-dependent solution at the interface.

We remark that, just as in the Toro-Titarev solver [35] reviewed in Sect. 2.2, the HEOC solution method as presented here applies to in-homogeneous non-linear conservation balance laws. The influence of the source term enters via the Cauchy-Kowalewski method, but note that at no point in the method it becomes necessary to solve Riemann problems, explicitly accounting for the influence of the source terms.

3.2 Interaction of Time Derivatives

Another method of solution for the DRP (1) results from a modification of both the Harten et al. (HEOC) and the Toro-Titarev (TT) solvers. The sought solution at the interface is again

expressed as in (3), with the leading term computed as in (6). This part is identical to the TT solver. To compute the higher order terms we solve *time-derivative* Riemann problems, that is, for any index $k > 0$ we compute $\partial_t^{(k)}\mathbf{Q}(0_-, 0)$ and $\partial_t^{(k)}\mathbf{Q}(0_+, 0)$ as in (20) (left) and (21) (right). To find $\partial_t^{(k)}\mathbf{Q}(0, 0_+)$ right at the interface we solve the classical linearized homogeneous Riemann problem

$$\left.\begin{array}{ll} \text{PDEs:} & \partial_t(\partial_t^{(k)}\mathbf{Q}(x,t)) + \mathbf{A}_{LR}^{(0)}\partial_x(\partial_t^{(k)}\mathbf{Q}(x,t)) = \mathbf{0}\ , \\ \text{ICs:} & \partial_t^{(k)}\mathbf{Q}(x,0) = \begin{cases} \partial_t^{(k)}\mathbf{Q}(0_-,0) & \text{if} \quad x < 0\ , \\ \partial_t^{(k)}\mathbf{Q}(0_+,0) & \text{if} \quad x > 0\ . \end{cases} \end{array}\right\} \tag{24}$$

The similarity solution is denoted by $\mathbf{T}^{(k)}(x/t)$ and the sought value is

$$\partial_t^{(k)}\mathbf{Q}(0, 0_+) = \mathbf{T}^{(k)}(0)\ . \tag{25}$$

The final solution has the form (11) with $\mathbf{C}_0$ as in (6) and

$$\mathbf{C}_k \equiv \frac{\partial_t^{(k)}\mathbf{Q}(0,0_+)}{k!} = \mathbf{T}^{(k)}(0)\ , \tag{26}$$

for $k = 1, \ldots, K$.

Note the analogy between (9) and (24). Both are motivated by the fact that for a linear homogeneous system with constant coefficient matrix $\hat{\mathbf{A}}$ all temporal and spatial partial derivatives of the vector of unknowns, if defined, obey the original system, namely

$$\left.\begin{array}{l} \partial_t(\partial_t^{(k)}\mathbf{Q}(x,t)) + \hat{\mathbf{A}}\partial_x(\partial_t^{(k)}\mathbf{Q}(x,t)) = \mathbf{0}\ , \\ \partial_t(\partial_x^{(k)}\mathbf{Q}(x,t)) + \hat{\mathbf{A}}\partial_x(\partial_x^{(k)}\mathbf{Q}(x,t)) = \mathbf{0}\ . \end{array}\right\} \tag{27}$$

Note also that for the DRP for the linear advection equation

$$\left.\begin{array}{ll} \text{PDE:} & \partial_t q + \lambda\partial_x q = 0\ ,\ \ x \in (-\infty, \infty)\ ,\ \ t > 0\ , \\ \text{IC:} & q(x,0) = \begin{cases} q_L(x) & \text{if} \quad x < 0\ , \\ q_R(x) & \text{if} \quad x > 0\ , \end{cases} \end{array}\right\} \tag{28}$$

with λ a constant wave propagation speed, all the proposed solutions (TT, HEOC, CT) coincide with the exact solution and is given by

$$q_{LR}(\tau) = \begin{cases} q_L(0_-) + \sum_{k=1}^{K}\left[(-1)^k\lambda^k q_L^{(k)}(0_-)\right]\dfrac{\tau^k}{k!} & \text{if} \quad \lambda > 0\ , \\ q_R(0_+) + \sum_{k=1}^{K}\left[(-1)^k\lambda^k q_R^{(k)}(0_+)\right]\dfrac{\tau^k}{k!} & \text{if} \quad \lambda < 0\ , \end{cases} \tag{29}$$

with

$$q_L^{(k)}(0_-) \equiv \frac{d^k}{dx^k}q_L(0_-)\ ,\ \ q_R^{(k)}(0_+) \equiv \frac{d^k}{dx^k}q_R(0_+)\ . \tag{30}$$

One can show that this is also true for a linear system with constant coefficients. For non-linear systems the theoretical justification of the proposed solution method remains an issue, as we shall point out in section 5. Obviously, for the special case of piece-wise constant data, the classical Riemann problem for non-linear systems is reproduced by all the methods studied.

In the next section we formulate high-order finite volume methods that are based on the solution of the DRP as the building block.

4 High-Order Numerical Schemes

The DRP solvers studied in this paper can be used to construct Godunov-type schemes of arbitrary order of accuracy. Here we consider these schemes in the framework of the finite volume method.

4.1 Finite Volume Schemes

The finite volume approach for a non-linear system of $m \times m$ hyperbolic equations with source terms

$$\partial_t \mathbf{Q} + \partial_x \mathbf{F}(\mathbf{Q}) = \mathbf{S}(\mathbf{Q}) \tag{31}$$

reads

$$\mathbf{Q}_i^{n+1} = \mathbf{Q}_i^n - \frac{\Delta t}{\Delta x}[\mathbf{F}_{i+\frac{1}{2}} - \mathbf{F}_{i-\frac{1}{2}}] + \Delta t \mathbf{S}_i \ , \tag{32}$$

where $\mathbf{Q}_i^n$ is an approximation to the spatial-integral average

$$\mathbf{Q}_i^n = \frac{1}{\Delta x} \int_{x_{i-\frac{1}{2}}}^{x_{i+\frac{1}{2}}} \mathbf{Q}(x, t^n) dx \tag{33}$$

in the volume $[x_{i-\frac{1}{2}}, x_{i+\frac{1}{2}}] \times [t^n, t^{n+1}]$. $\mathbf{F}_{i+\frac{1}{2}}$ is the numerical flux, which is an approximation to the time-integral average (2), and $\mathbf{S}_i$ is the numerical source, which is an approximation to a volume integral. The numerical scheme is completely defined once expressions for $\mathbf{F}_{i+\frac{1}{2}}$ and $\mathbf{S}_i$ are provided.

In the ADER method the numerical flux $\mathbf{F}_{i+\frac{1}{2}}$ is computed by solving the Derivative Riemann Problem

$$\left.\begin{array}{rl} \text{PDEs:} & \partial_t \mathbf{Q} + \partial_x \mathbf{F}(\mathbf{Q}) = \mathbf{S}(\mathbf{Q}) \ , \\ \text{IC:} & \mathbf{Q}(x,0) = \left\{ \begin{array}{lll} \mathbf{P}_i(x) & \text{if} & x < 0 \ , \\ \mathbf{P}_{i+1}(x) & \text{if} & x > 0 \ , \end{array} \right. \end{array}\right\} \tag{34}$$

and then computing the time average as in (2). Here $\mathbf{P}_i(x)$ is a vector defined in cell $[x_{i-\frac{1}{2}}, x_{i+\frac{1}{2}}]$ whose components are reconstructed polynomials of an appropriate degree; likewise $\mathbf{P}_{i+1}(x)$. In principle, any reconstruction procedure can be used but in practice the non-linear ENO and WENO reconstruction procedures are recommended [11], [26], [25]. The DRP (34) can be solved using any of the methods studied in this paper.

In the ADER approach the numerical source $\mathbf{S}_i$ results from a high-order approximation to the volume-integral average

$$\mathbf{S}_i = \frac{1}{\Delta t} \frac{1}{\Delta x} \int_0^{\Delta t} \int_{x_{i-\frac{1}{2}}}^{x_{i+\frac{1}{2}}} \mathbf{S}(\mathbf{Q}_i(x,t)) dx dt \ , \tag{35}$$

still denoted by $\mathbf{S}_i$, where $\mathbf{Q}_i(x,t)$ is a high-order approximation to the solution of (31) inside the control volume, obtained as follows. At any point $x_d \in [x_{i-\frac{1}{2}}, x_{i+\frac{1}{2}}]$ the solution $\mathbf{Q}(x_d,\tau)$, as a function of time, is computed using the Cauchy-Kowalewski method,

$$\mathbf{Q}(x_d,\tau) = \mathbf{Q}(x_d,0) + \sum_{k=1}^{K} \left[\partial_t^{(k)} \mathbf{Q}(x_d,0)\right] \frac{\tau^k}{k!} . \tag{36}$$

The functions $\mathbf{G}^{(k)}$ in (7) are now functions of space derivatives of the reconstruction polynomial $\mathbf{P}_i(x)$ and thus

$$\mathbf{Q}_i(x_d,\tau) = \mathbf{P}_i(x_d) + \sum_{k=1}^{K} \left[\mathbf{G}^{(k)}(\mathbf{P}_i^{(0)}(x_d), \mathbf{P}_i^{(1)}(x_d), \ldots, \mathbf{P}_i^{(k)}(x_d))\right] \frac{\tau^k}{k!} . \tag{37}$$

With this information available the space-time integral average can be computed to any desired order of accuracy.

4.2 Analogy with Second-Order Schemes

The second order version of the ADER schemes reported in [31] is analogous to the GRP scheme of Ben-Artzi and Falcovitz [1]. In fact the scheme of [31] is a modification of the GRP scheme, whereby the computation of the time derivative in the power series expansion (to second order) for the solution of the DRP is reduced to computing the solution of a linearized Riemann problem for spatial gradients. The higher order ADER schemes are a straight generalization of this modified GRP scheme. As seen in previous sections, the numerical flux is computed at the solution of the Derivative Riemann Problem at the interface, which is found as a power series expansion right at the interface $x = 0$, as a function of time.

Similarly, the method of Harten et al. [10] in its second-order mode may be seen as a way of interpreting the second order MUSCL-Hancock scheme [38], the numerical flux of which is

$$\mathbf{F}_{i+\frac{1}{2}}^{MH} = \mathbf{F}_{i+\frac{1}{2}}^{MH}(\tilde{\mathbf{Q}}_i^R, \tilde{\mathbf{Q}}_{i+1}^L) = \mathbf{F}(\tilde{\mathbf{Q}}_{i+\frac{1}{2}}(0)) , \tag{38}$$

where $\tilde{\mathbf{Q}}_{i+\frac{1}{2}}(x/t)$ is the similarity solution of the classical Riemann problem

$$\left.\begin{array}{lll} \text{PDEs:} & \partial_t \mathbf{Q} + \partial_x \mathbf{F}(\mathbf{Q}) = \mathbf{0} , & x \in (-\infty,\infty) , \quad t > 0 , \\ \text{IC:} & \mathbf{Q}(x,0) = \left\{ \begin{array}{ll} \tilde{\mathbf{Q}}_i^R & \text{if} \quad x < 0 , \\ \tilde{\mathbf{Q}}_{i+1}^L & \text{if} \quad x > 0 , \end{array} \right. & \end{array}\right\} \tag{39}$$

with

$$\left.\begin{array}{rcl} \tilde{\mathbf{Q}}_i^R & = & \mathbf{Q}_i^R - \frac{1}{2}\frac{\Delta t}{\Delta x}[\mathbf{F}(\mathbf{Q}_i^R) - \mathbf{F}(\mathbf{Q}_i^L)] , \\ \tilde{\mathbf{Q}}_{i+1}^L & = & \mathbf{Q}_{i+1}^L - \frac{1}{2}\frac{\Delta t}{\Delta x}[\mathbf{F}(\mathbf{Q}_{i+1}^R) - \mathbf{F}(\mathbf{Q}_{i+1}^L)] \end{array}\right\} \tag{40}$$

and

$$\mathbf{Q}_i^R = \mathbf{Q}_i^n + \frac{1}{2}\Delta x \mathbf{\Delta}_i , \quad \mathbf{Q}_{i+1}^L = \mathbf{Q}_{i+1}^n - \frac{1}{2}\Delta x \mathbf{\Delta}_{i+1} . \tag{41}$$

Here $\mathbf{\Delta}_i$ and $\mathbf{\Delta}_{i+1}$ are the slopes in the MUSCL reconstruction in cells i and $i+1$ respectively. Note the relation

$$\mathbf{\Delta}_i = \frac{\mathbf{Q}_i^R - \mathbf{Q}_i^L}{\Delta x} = \mathbf{P}_i' , \quad \mathbf{\Delta}_{i+1} = \frac{\mathbf{Q}_{i+1}^R - \mathbf{Q}_{i+1}^L}{\Delta x} = \mathbf{P}_{i+1}' . \tag{42}$$

On the other hand, a second-order method with the HEOC solver, see (13)-(14), has flux

$$\mathbf{F}_{i+\frac{1}{2}} = \mathbf{F}_{i+\frac{1}{2}}\left(\tilde{\mathbf{Q}}_L(\frac{1}{2}\Delta t), \tilde{\mathbf{Q}}_R(\frac{1}{2}\Delta t)\right) = \mathbf{F}\left(\mathbf{D}(\frac{1}{2}\Delta t, 0)\right) \ . \tag{43}$$

See (22). From (13) and (14) we have

$$\left.\begin{array}{l} \tilde{\mathbf{Q}}_L(\frac{1}{2}\Delta t) = \mathbf{P}_i(0_-) - \frac{1}{2}\Delta t \mathbf{A}_L \mathbf{P}_i'(0_-) \ , \\ \\ \tilde{\mathbf{Q}}_R(\frac{1}{2}\Delta t) = \mathbf{P}_{i+1}(0_+) - \frac{1}{2}\Delta t \mathbf{A}_R \mathbf{P}_{i+1}'(0_+) \ , \end{array}\right\} \tag{44}$$

with

$$\mathbf{A}_L = \mathbf{A}(\mathbf{Q}_L(0_-)) \ , \quad \mathbf{A}_R = \mathbf{A}(\mathbf{Q}_R(0_+)) \ . \tag{45}$$

For a linear system with constant coefficient matrix $\hat{\mathbf{A}}$ we have $\mathbf{F}(\mathbf{Q}) = \hat{\mathbf{A}}\mathbf{Q}$ and one sees that the left and right states in (39) are identical to those in (44) and thus the second order ADER scheme based on the HEOC solver is identical to the MUSCL-Hancock scheme.

The schemes are not identical for non-linear systems but the analogy just discussed provides an interpretation to the rather *enigmatic* evolution step (40) of the boundary extrapolated values by half a time step, in the MUSCL-Hancock method.

Thus, from the numerical point of view, we can interpret the numerical method of Harten et al. [10] as being a high-order generalization of the MUSCL-Hancock second order method. Similarly, the ADER method, with any of the DRP solvers studied here, may be interpreted as a high-order generalization of the second order method of Ben-Artzi and Falcovitz [1], following its modification reported in [31].

Corresponding finite volume schemes in two space dimensions using unstructured meshes are described in Sect. 6.

5 Tests for the Derivative Riemann Problem Solvers

In this section we assess the performance of the Derivative Riemann Problem solvers studied in the paper via a series of test problems for the Euler equations of gas dynamics. As no exact solutions are known for the class of test problems of interest here, we obtain reference solutions by computing solutions numerically. To this end we use three numerical methods, the first-order Godunov method, the second-order MUSCL-Hancock method and the Random Choice Method (RCM) [8], all of them applied on a very fine mesh.

We note that RCM has the unique property of being able to resolve the very-early time evolution of the solution in a way that no other method known to us can do. This is important, as the proposed DRP solvers are assessed in their domain of validity, namely for short times. For test problems involving an initial discontinuity, most methods will require a fairly large number of time steps to begin to gradually establish the structure of the true solution. Moreover, the early-time numerical results may exhibit large unphysical oscillations, even when monotone (for the scalar case) schemes are used. To illustrate this point we solve a simple shock-tube problem in the domain $[-1, 1]$, with initial data $\rho_L = 1$, $u_L = 3/4$, $p_L = 1$ for $x < 0$ and $\rho_R = 1/8$, $u_R = 0$, $p_R = 1/10$ for $x > 0$.

Fig. 4 shows the exact (full line) and numerical solutions (symbols) at time $t = 0.015$ using the the Godunov first-order method (circles), the MUSCL-Hancock method (squares) and the RCM method (triangles). For all three numerical methods we use the exact Riemann solver. For the first two methods we use $C_{cfl} = 0.9$ and for RCM we use $C_{cfl} = 0.45$. Fig. 4 shows

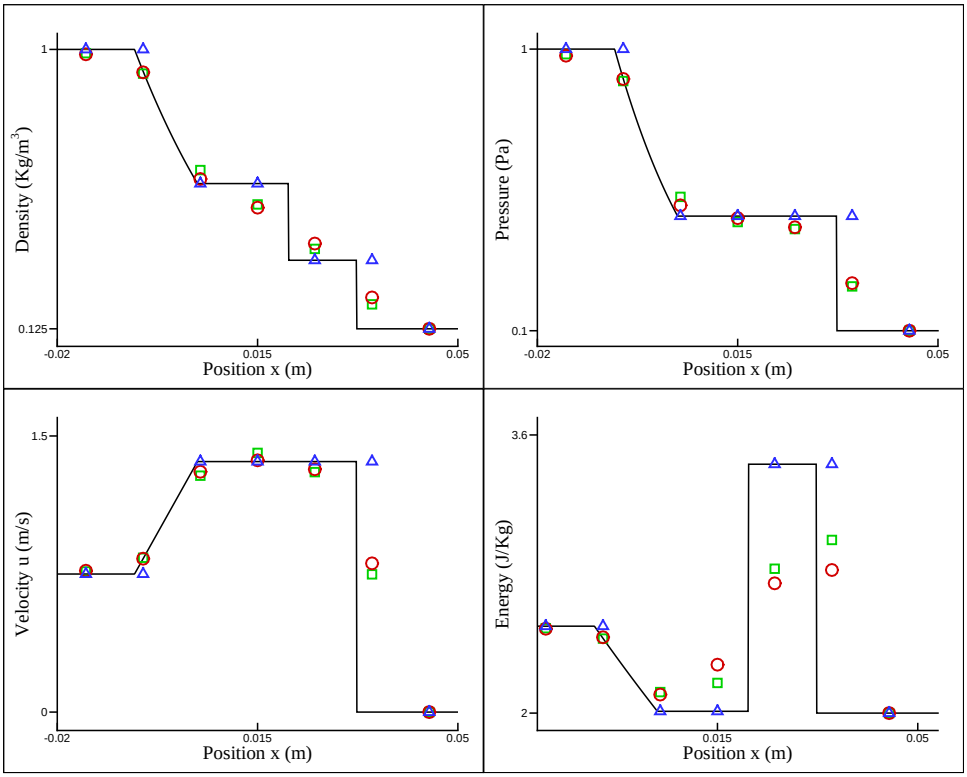

Figure 4: Shock-tube test problem. Exact (full line) and numerical solutions (symbols) at time $t = 0.015$ using the Godunov first-order method (circles), the MUSCL-Hancock method (squares) and the random choice method (triangles).

only the region close to the position of the discontinuities at time $t = 0$. For the output time considered the Godunov and MUSCL-Hancock methods do only four time steps and RCM nine time steps. The first two methods are unable to resolve the wave structure correctly. RCM finds all intermediate states correctly. This property of RCM is useful to our purpose.

Recall that the DRP solution is valid precisely at the interface $x = 0$, as a function of time. The numerical methods give the approximate solution in every cell of the mesh that discretizes the domain $[-1, 1]$. For any mesh used one always has, at any time, one value (vector) immediately to the left of $x = 0$ and one immediately to the right of $x = 0$. To extract the sought reference solution at a given time we solve the classical Riemann problem for these two neighbouring states and pick up the solution right at the interface $x = 0$. This is the *numerical* solution that we compare with the DRP solutions.

The series of test problems includes a simple test (Test 1) with smooth initial condition throughout, no discontinuities in the data are present. A second test (Test 2) has no jump discontinuities in the state variables but admits discontinuities in derivatives at the interface. Other more demanding test problems are constructed from Test 2, by adding a discontinuity in pressure. Four new cases are thus generated by varying the strength of the initial pressure jump $\Delta p = (p_L - p_R)/p_R$ at the interface, namely $\Delta p = 0.01$, $\Delta p = 0.1$, $\Delta p = 1.0$ and $\Delta p = 10.0$. For these four cases with an initial jump discontinuity the reference numerical solution used is that obtained by the Random Choice Method, on a very fine mesh.

5.1 Test 1: smooth initial conditions

The initial conditions, given in (46), are smooth throughout, there are no jumps in state or derivatives at $x = 0$. In this particular case all three DRP solvers give, algebraically, the same solution.

$$\left.\begin{array}{ll} \rho(x,0) & = 1 + \frac{4}{5}sin(\frac{\pi x}{2}) + \frac{1}{10}sin(\frac{5\pi x}{2}) \\ u(x,0) & = \frac{1}{2}(x - \frac{1}{2})^4 \\ p(x,0) & = 10 + 2x^4 \end{array}\right\} \tag{46}$$

In Fig. 5 we present the solution of the DRP problem up to fifth order (DRP 4) for all three components of the vector $\mathbf{Q} = [\rho, \rho u, E] \equiv [\mathbf{Q}(1), \mathbf{Q}(2), \mathbf{Q}(3)]$, where ρ is density, u is particle velocity and E is total energy. As expected, by increasing the order, the DRP solution approximates the reference solution very well. The DRP_0 solution is constant in time and the DRP_1 solution is linear in time. We note that the approximation improves with the order, which is verified for all three components $\mathbf{Q}(1)$, $\mathbf{Q}(2)$ and $\mathbf{Q}(3)$. For $\mathbf{Q}(2)$ the DRP 1 solution is practically identical to the DRP_0 solution. This is correct in the sense that at the time $\tau = 0^+$ the slope of the reference solution is close to zero and the linear characteristic of the DRP 1 solution will not modify this slope. Table 1 shows the error in the L_2 norm at different times. The main feature of these errors is that as time decreases the error decreases and as the order of accuracy increases the error decreases, as expected.

5.2 Test 2: Initial data with discontinuous derivatives

Test 2 has piece-wise smooth initial conditions that are continuous at $x = 0$ but with discontinuous derivatives at $x = 0$, see (47). For this test problem all three DRP solvers (TT, CT and HEOC) agree quite well for the very early times but differ quite visibly for larger times. Figure 6 shows the fifth-order (DRP_4) solution for the three solvers, for each component of the vector $\mathbf{Q}$. For the first and third components the solver CT is the most accurate, followed by HEOC. For the second component of $\mathbf{Q}$, the TT solver gives better results. More comprehensive

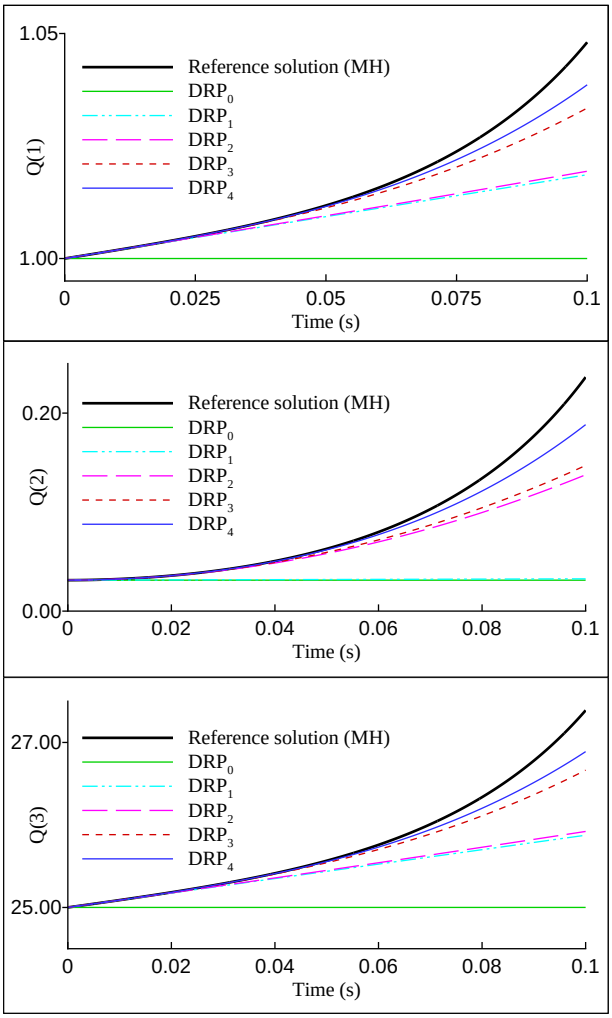

Figure 5: Test 1: DRP solution for $Q(1) = \rho$, $Q(2) = \rho u$ and $Q(3) = E$. Thick line is the reference solution.

Order	$t = 0.0125$	$t = 0.0250$	$t = 0.0500$	$t = 0.1000$
DRP_0	1.11656×10^{-1}	2.34541×10^{-1}	5.67043×10^{-1}	$2.39794 \times 10^{+0}$
DRP_1	2.79222×10^{-3}	1.70783×10^{-2}	1.32228×10^{-1}	$1.52756 \times 10^{+0}$
DRP_2	1.51932×10^{-3}	1.27545×10^{-2}	1.17151×10^{-1}	$1.47129 \times 10^{+0}$
DRP_3	6.89536×10^{-5}	1.15772×10^{-3}	2.44542×10^{-2}	7.30551×10^{-1}
DRP_4	1.32762×10^{-5}	2.66533×10^{-4}	1.02054×10^{-2}	5.02807×10^{-1}

Table 1: Errors in L_2 norm for the vector $\mathbf{Q}$ for Test 1.

information about the relative merits of the three solvers is given in Tables 2 to 4, where errors measured in the L_2 norm are displayed. For time $t = 0.0250$, the error of the DRP_4 solution for the TT solver is 1.3295584×10^{-2}, for the HEOC solver is 7.3686016×10^{-3} and for the CT solver is 5.1386851×10^{-3}. A general conclusion is that for all three solvers the error diminishes as the order increases, while the solution is more accurate for small times, and for which they all tend to agree.

$$\left.\begin{array}{rcl} \rho_L(x,0) & = & 1.433903078 + \frac{4}{5}sin(\frac{\pi(x-0.3)}{2}) + \frac{1}{10}sin(\frac{5\pi(x-0.3)}{2}) \\ u_L(x,0) & = & \frac{1}{2}(x-\frac{4}{5})^4 - 0.17355 \\ p_L(x,0) & = & 9.9838 + 2(x-0.3)^4 \\ \rho_R(x,0) & = & 1 + \frac{4}{5}sin(\frac{\pi x}{2}) + \frac{1}{10}sin(\frac{5\pi x}{2}) \\ u_R(x,0) & = & \frac{1}{2}(x-\frac{1}{2})^4 \\ p_R(x,0) & = & 10 + 2x^4 \end{array}\right\} \quad (47)$$

Order	$t = 0.0125$	$t = 0.0250$	$t = 0.0500$	$t = 0.1000$
DRP_0	3.18474×10^{-1}	6.99227×10^{-1}	$1.76165 \times 10^{+0}$	7.85676×10^{0}
DRP_1	2.43169×10^{-2}	1.11019×10^{-1}	5.85425×10^{-1}	5.50450×10^{0}
DRP_2	3.57148×10^{-3}	2.80474×10^{-2}	2.53714×10^{-1}	4.17824×10^{0}
DRP_3	1.98152×10^{-3}	1.53861×10^{-2}	1.52705×10^{-1}	3.36836×10^{0}
DRP_4	1.85090×10^{-3}	1.32955×10^{-2}	1.19316×10^{-1}	2.83279×10^{0}

Table 2: Toro-Titarev solver. Errors for Test 2.

Order	$t = 0.0125$	$t = 0.0250$	$t = 0.0500$	$t = 0.1000$
DRP_0	3.18474×10^{-1}	6.99227×10^{-1}	$1.76165 \times 10^{+0}$	7.85676×10^{0}
DRP_1	2.46867×10^{-2}	1.12490×10^{-1}	5.91241×10^{-1}	5.52721×10^{0}
DRP_2	4.70401×10^{-3}	3.29470×10^{-2}	2.76097×10^{-1}	4.29057×10^{0}
DRP_3	1.78129×10^{-3}	9.56147×10^{-3}	8.91781×10^{-2}	2.79727×10^{0}
DRP_4	1.64408×10^{-3}	7.36860×10^{-3}	5.42299×10^{-2}	2.25443×10^{0}

Table 3: HEOC solver: Errors for Test 2.

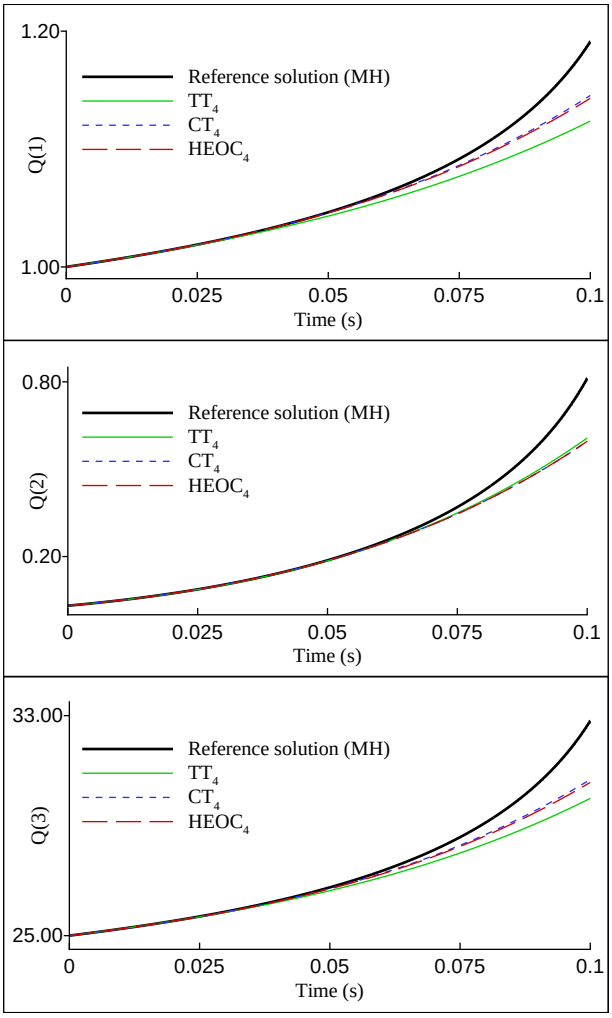

Figure 6: Fifth order DRP solutions for Test 2, using TT, CT and HEOC for the three components of Q.

5.3 Tests with discontinuous initial conditions

The tests of this section are generated from the initial conditions of Test 2 by adding a term in $p_L(x,0)$ and thus generating a jump $\Delta p = (p_L(0,0) - p_R(0,0))/p_R(0,0)$ in pressure at $x = 0$. We consider the four cases: $\Delta p = 0.01, 0.1, 1.0, 10.0$.

Results are shown in Figures 7 to Figure 10. Figure 7 displays results for $\Delta p = 0.01$, with a small pressure jump; the DRP solution improves as the order increases, for all three solvers. In Fig. 8, for $\Delta p = 0.10$, the solution from the TT solver improves as the order increases. The situation is different for the CT and HEOC solvers, whose solutions cross the reference solution.

Results for $\Delta p = 1.00$ are shown in Fig. 9. Here the Toro-Titarev solver seems to perform better but note that when the order increases to DRP_4, it misrepresents the curvature and thus crosses the reference solution. The solutions of the present solvers CT and HEOC show wrong initial slopes. As the order increases the curvature seems to approximate the curvature of the reference solution better, with the HEOC solution being closer to the reference solution than that of CT. For both the CT and HEOC solvers the second order solution crosses the reference solution.

Figure 10 shows the DRP solutions for $\Delta p = 10.0$. All three solvers give the wrong initial slope. Their failure to agree with the reference solution increases dramatically as the initial pressure jump becomes larger. Moreover, they fail to capture the initial slope and the behaviour of the reference solution.

5.4 Discussion of results

Recall that the main purpose of solving the Derivative Riemann Problem (DRP) is to provide a time-dependent solution at each cell interface, from which a corresponding numerical flux can be found and used in the context of finite volume methods or discontinuous Galerkin finite element methods. However, before considering numerical methods we focus the discussion on the solution of the particular Cauchy problem, the DRP. There are a number of aspects of the solution procedure of the DRP that warrant a detailed discussion.

One issue concerns the time evolution of the initial data, as done in the HEOC solver, and of the solution, as done in the TT and CT solvers. We have observed that even when the initial condition consists of physically admissible data, it is possible that the time evolution yields unphysical values, such as negative densities. This appears to be more crucial for the HEOC solver, because it could happen that, at a given time, the time evolved data contains unphysical values, which then the appropriate (classical) Riemann solver rejects, leading to a failure of the scheme. The TT and CT solvers appear to be less sensitive to this problem. These two solvers evolved in time the sought solution right at the interface. The corresponding time-dependent solution may still include unphysical values. However, since these are then only used in the

Order	$t = 0.0125$	$t = 0.0250$	$t = 0.0500$	$t = 0.1000$
DRP_0	3.18474×10^{-1}	6.99227×10^{-1}	$1.76165 \times 10^{+0}$	7.85676×10^{0}
DRP_1	2.43169×10^{-2}	1.11019×10^{-1}	5.85425×10^{-1}	5.50450×10^{0}
DRP_2	4.24609×10^{-3}	3.07728×10^{-2}	2.64623×10^{-1}	4.22135×10^{0}
DRP_3	1.32223×10^{-3}	7.34350×10^{-3}	7.70900×10^{-2}	2.72215×10^{0}
DRP_4	1.18530×10^{-3}	5.13868×10^{-3}	4.14296×10^{-2}	2.14972×10^{0}

Table 4: CT (present) solver. Errors for Test 2.

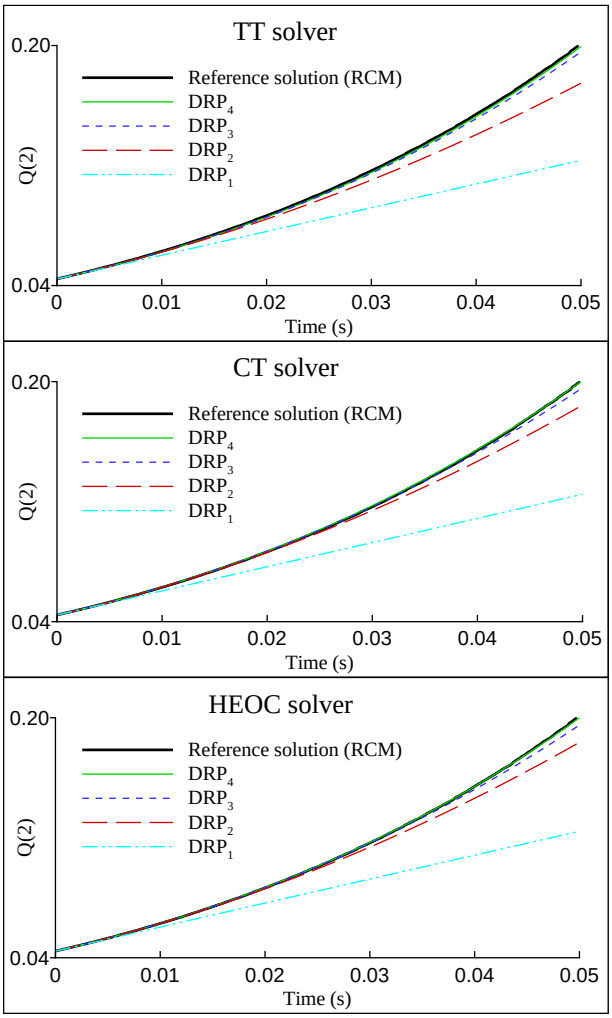

Figure 7: DRP solution for TT, CT and HEOC solvers for $\Delta p = 0.01$. Thick full line is the reference solution obtained with RCM method.

numerical integration to obtain the flux it is possible that the scheme may continue to function.

Stationary discontinuities in the solution of the DRP represent another situation where differences between the various solvers exist. The TT and CT solvers expand the solution at the interface starting from a leading term computed a time $t = 0_+$ that dominates the evolution. In the presence of a stationary discontinuity at $t = 0_+$ there are two possible choices for the leading term. For the first-order mode of the methods, it does not matter which of the two states is taken, as these satisfy the Rankine-Hugoniot conditions and therefore the respective fluxes are identical. For the higher-order version of the methods the situation is not clear. There will be two different time expansions, depending on which side is taken as the leading term. This non-uniqueness remains so even if the discontinuity moves for times $t > 0$. We have performed some numerical tests on the effect of choosing from the two available expansions. There is an observable numerical difference but, at least for the tests performed, it is very small and as time evolves it virtually vanishes. Still, this is an aspect of the TT and CT methods that would benefit from further investigations. On the other hand, the HEOC method is less sensitive to this problem. In particular, if the discontinuity positioned at the origin, at the early times, then moves as time increases. The the HEOC has the mechanism to capture this behaviour.

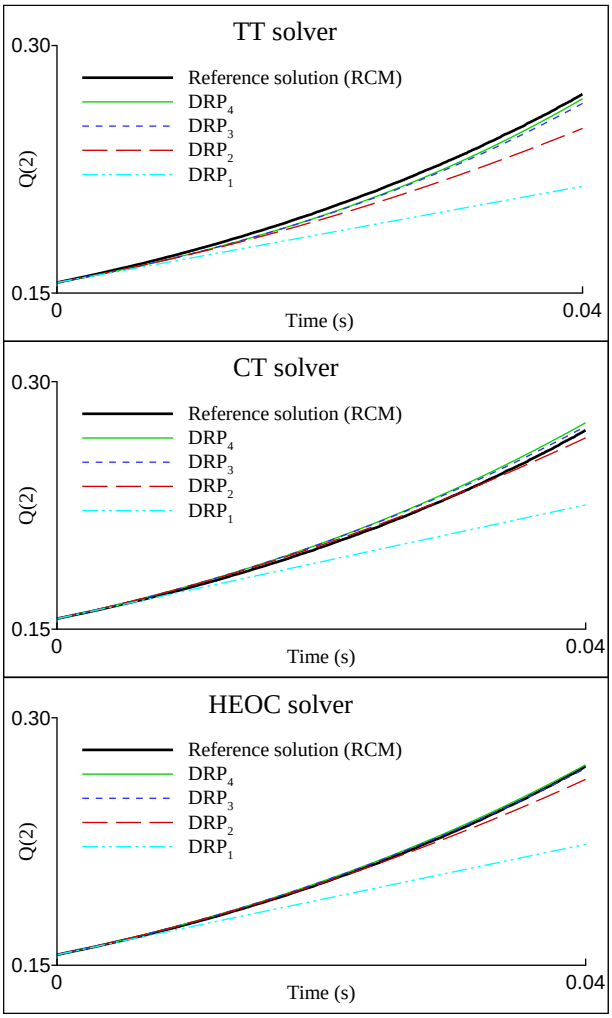

Figure 8: DRP solution for TT, CT and HEOC solvers for $\Delta p = 0.10$. Thick full line is the reference solution obtained with RCM method.

In general, boundary conditions are a challenging problem in the context of high order numerical methods. For example, for reflecting boundary conditions we *solve* an inverse Riemann problem, in the sense that we need to identify appropriate initial conditions such that the Riemann problem solution at the boundary reproduces what is physically sought, for example, zero velocity. To this purpose the HEOC solver appears more attractive than the TT and CT solvers, as it is very simple to create, at each time, in the time evolution process, the appropriate data states to match the desired condition.

Some comments regarding computational cost are in order. The HEOC solver needs a *robust* Riemann solver for each *time-integration point* τ, within the time step $0 \leq \tau \leq \Delta t$. This can be time-consuming as a robust Riemann solver will in general be a non-linear Riemann solver. In addition, the HEOC solver requires the development of two series expansions, one on each side of the interface. The TT solver, on the other hand, requires a single expansion right at the interface. Moreover, in the TT and CT solvers, one uses a non-linear Riemann solver only once, in order to compute the leading term reliably.

A rather surprising observation resulting from the present work is that, from the evidence available, all three DRP solvers are unable to resolve correctly the DRP problem for the case

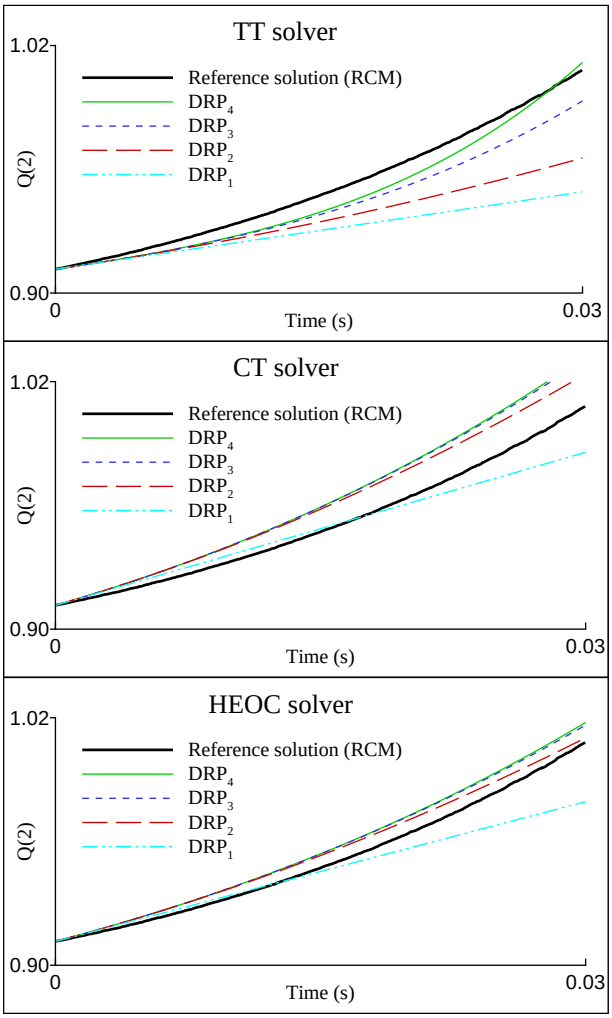

Figure 9: DRP solution for TT, CT and HEOC solvers for $\Delta p = 1.00$. Thick full line is the reference solution obtained with RCM method.

of *non-linear systems with large jumps*. This is different from the case of scalar non-linear problems. In fact, it has been demonstrated that the TT solver [33] gives the correct solution for the non-linear Burgers equation, even with a non-linear source term, for initial jumps of any size. This property does not seem to carry to systems (non-linear). Recall that for linear systems all methods are equivalent and all give the correct solution.

On the other hand, the available experience shows that the high order ADER schemes based on the solution of the Derivative Riemann Problem are capable of producing the theoretically expected orders of accuracy. Obviously, the corresponding convergence rate tests are performed for smooth solutions. However, even for smooth solutions the local reconstruction procedure will necessarily produce jumps at the interfaces. Obviously these jumps are small, and possibly within the range that allows the existing DRP solvers to resolve correctly.

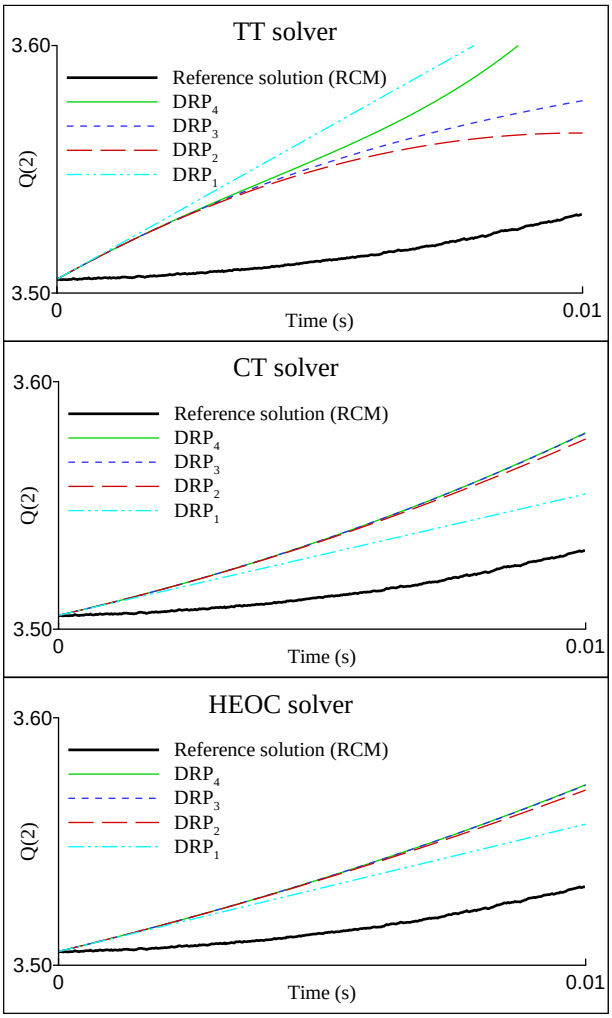

Figure 10: DRP solution for TT, CT and HEOC solvers for $\Delta p = 10.0$. Thick full line is the reference solution obtained with RCM method.

6 ADER Methods on Triangular Meshes

The purpose of this section is to briefly outline the procedure to construct high-order finite volume methods on unstructured meshes and to illustrate the way the solution of the Derivative Riemann Problem can be used as the building block for such numerical schemes. We restrict ourselves to two space dimensions and study two problems. The first one is used to carry out a convergence rate study and to show that the theoretically expected high order accuracy is actually verified in practice, at least for the chosen test problem. The second test is used to illustrate the fact that the proposed schemes can be used to solve realistic problems involving shock waves on complicated, non-cartesian geometries.

6.1 Equations and Finite Volume Schemes

We solve the two-dimensional compressible Euler equations

$$\frac{\partial}{\partial t}\mathbf{Q} + \frac{\partial}{\partial x}\mathbf{F}(\mathbf{Q}) + \frac{\partial}{\partial y}\mathbf{G}(\mathbf{Q}) = \mathbf{0}, \tag{48}$$

with

$$\mathbf{Q} = \begin{pmatrix} \rho \\ \rho u \\ \rho v \\ E \end{pmatrix}, \ \mathbf{F}(\mathbf{Q}) = \begin{pmatrix} \rho u \\ \rho u^2 + p \\ \rho uv \\ u(E+p) \end{pmatrix}, \ \mathbf{G}(\mathbf{Q}) = \begin{pmatrix} \rho v \\ \rho uv \\ \rho v^2 + p \\ v(E+p) \end{pmatrix}, \tag{49}$$

and the ideal equation of state, with the specific internal energy given as $e(\rho, p) = \frac{p}{\rho(\gamma-1)}$. Here ρ is density, u, v are x and y components of velocity, p is pressure and E is the total energy, defined as $E = \rho(\frac{1}{2}(u^2+v^2) + e(\rho, p))$. For the calculations of this paper we take $\gamma = 1.4$, as for air.

The schemes are constructed by considering a control volume T_m in a two-dimensional domain, where T_m is an element of a conformal triangulation of the full spatial domain Ω. Writing equations (48) in divergence form

$$\mathbf{Q}_t + \nabla \mathbf{H}(\mathbf{Q}) = \mathbf{0} \ , \ \ \mathbf{H}(\mathbf{Q}) = [\mathbf{F}(\mathbf{Q}), \mathbf{G}(\mathbf{Q})]^T \tag{50}$$

and integrating over the triangle in space and time we obtain

$$\mathbf{Q}_m^{n+1} = \mathbf{Q}_m^n - \frac{\Delta t}{|T_m|} \sum_{j=1}^{3} \mathbf{H}_{m,j}^n \ . \tag{51}$$

Here $\mathbf{H}_{m,j}^n$ is the numerical flux across the edge j of the triangle T_m, $|T_m|$ is the area of triangle T_m and $\mathbf{Q}_m^n$ is the cell average

$$\mathbf{Q}_m^n = \frac{1}{|T_m|} \int_{T_m} \mathbf{Q}(\mathbf{x}, t^n) d\mathbf{x} \ . \tag{52}$$

Once the numerical flux across the edges of the triangle are defined we obtain an explicit one step numerical method. The numerical flux $\mathbf{H}_{m,j}^n$ for edge j is obtained by integrating along the edge $\partial T_{m,j}$ in the time interval $[t^n, t^{n+1}]$,

$$\mathbf{H}_{m,j}^n \ = \ \frac{1}{\Delta t} \int_{t^n}^{t^{n+1}} \int_{\partial T_{m,j}} \mathbf{F}(\mathbf{Q}(\mathbf{x}, \tau)) \cdot \mathbf{n} \ \ d\mathbf{x} \ d\tau \ , \tag{53}$$

which is approximated as

$$\mathbf{H}_{m,j}^n \ = \ \sum_{k=1}^{N^t} \omega_k^t \, |\partial T_{m,j}| \sum_{h=1}^{N^x} \omega_h^x \ \ \mathbf{F}(\mathbf{Q}(\boldsymbol{x}_h, t_k)) \cdot \mathbf{n} \ . \tag{54}$$

The integration (53) is obtained by a Gaussian quadrature of the desire order defining the quadrature points $\boldsymbol{x}_h$ and t_k and the weights ω_h^x and ω_k^t, with $\boldsymbol{x}_h \in \partial T_{m,j}$ and $t_k \in [t^n, t^{n+1}]$. At each spatial integration point $\boldsymbol{x}_h$ we set locally a Derivative Riemann Problem (1) to obtain the vector $\mathbf{Q}(\boldsymbol{x}_h, t_k) = \mathbf{Q}_{LR}(t_k)$ as in (3), see Fig. 11. $\mathbf{Q}_{LR}(\tau)$ can be obtained by using any of the three DRP solvers studied in this paper. Recall that the basic information available in finite volume schemes is a set of cell averages and therefore in order to produce a high order representation of the data in each cell we need to perform a reconstruction procedure to obtain the data for (1). Here we apply the reconstruction procedure reported in [6], which extends the ideas of the ENO/WENO techniques [13] combined with the sectorial stencil of [16] and the use of orthogonal basis functions from the discontinuous Galerkin methodology.

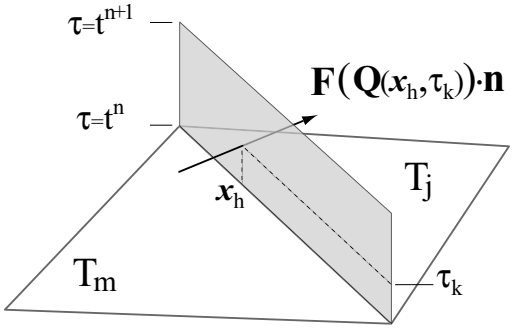

Figure 11: Numerical flux computed at the Gaussian point $x = x_h$ and $t = t_k$.

6.2 Convergence rate studies

For the purpose of studying the convergence rates of the schemes we adopt the test problem proposed in [12], which consists of a convected isentropic vortex computed in a square domain, with periodic boundary conditions. The initial condition consists of a mean constant flow modified by an isentropic perturbation. The initial mean flow is given by $\rho = 1$, $p = 1$ and $(u, v) = (1, 1)$ and the perturbation is given by

$$\left.\begin{aligned} \delta u &= -\frac{\epsilon}{2\pi} e^{\frac{1}{2}(1-r^2)y}, \\ \delta v &= \frac{\epsilon}{2\pi} e^{\frac{1}{2}(1-r^2)x}, \\ \delta \rho &= (1+\delta T)^{\frac{1}{\gamma-1}} - 1, \\ \delta p &= (1+\delta T)^{\frac{\gamma}{\gamma-1}} - 1, \\ \delta T &= -\frac{(\gamma-1)\epsilon^2}{8\gamma\pi^2} e^{1-r^2}, \end{aligned}\right\} \tag{55}$$

where $r^2 = x^2 + y^2$, $\epsilon = 5$ (the vortex strength) and γ is taken as $\gamma = 1.4$. The computational domain is $[-5, 5] \times [-5, 5]$ discretized by an unstructured mesh of triangles.

Tables 5 to 8 give errors and convergence rates for the finite volume ADER schemes using the CT (present) derivative Riemann problem solver. Schemes up to fifth order of accuracy are considered, on four levels of mesh refinement. Errors are measured in three norms L_1, L_2, L_∞ and the corresponding empirical orders of accuracy are O_1, O_2 and O_∞. The expected orders of accuracy are reached in all cases.

Mesh	L_1 error	O_1	L_2 error	O_2	L_∞ error	O_∞
224	2.47×10^{00}		5.67×10^{-1}		4.43×10^{-1}	
898	1.42×10^{00}	0.85	3.42×10^{-1}	0.78	2.82×10^{-1}	0.69
3618	3.43×10^{-1}	2.03	8.19×10^{-2}	2.04	8.71×10^{-2}	1.67
14402	5.84×10^{-2}	2.56	1.37×10^{-2}	2.58	1.51×10^{-2}	2.53
57694	7.65×10^{-3}	2.99	1.37×10^{-3}	3.11	4.22×10^{-3}	1.88

Table 5: Convergence rates test: second order method.

Mesh	L_1 error	O_1	L_2 error	O_2	L_∞ error	O_∞
224	2.29×10^{00}		5.23×10^{-1}		4.11×10^{-1}	
898	7.35×10^{-1}	1.75	1.65×10^{-1}	1.77	1.30×10^{-1}	1.77
3618	1.02×10^{-1}	2.82	2.49×10^{-2}	2.70	1.94×10^{-2}	2.71
14402	1.60×10^{-2}	2.67	4.03×10^{-3}	2.63	2.84×10^{-3}	2.78
57694	2.06×10^{-3}	3.02	5.21×10^{-4}	3.01	3.64×10^{-4}	3.03

Table 6: Convergence rates test: third order method.

Mesh	L_1 error	O_1	L_2 error	O_2	L_∞ error	O_∞
224	2.14×10^{00}		4.87×10^{-1}		3.88×10^{-1}	
898	3.76×10^{-1}	2.68	6.23×10^{-2}	3.17	5.03×10^{-2}	3.14
3618	1.67×10^{-2}	4.43	3.50×10^{-3}	4.10	3.87×10^{-3}	3.65
14402	1.12×10^{-3}	3.91	2.25×10^{-4}	3.97	2.48×10^{-4}	3.97
57694	6.84×10^{-5}	4.12	1.37×10^{-5}	4.12	1.61×10^{-5}	4.03

Table 7: Convergence rates test: fourth order method.

6.3 Shock wave reflection problem

The purpose of this test is simply to illustrate the potential of the methods presented to solve realistic problems to high accuracy on complicated domains discretized with unstructured meshes. To this end we consider the reflection of a shock wave from a solid body of triangular shape. The two-dimensional computational domain is the region $[-0.65, 0.5] \times [-0.5, 0.5]$, with a triangular solid body defined by the positions of its vertexes $v_1 = (-0.2, 0)$, $v_2 = (0.1, -1/6)$ and $v_3 = (0.1, 1/6)$. The incident shock wave has shock Mach number $Ms = 1.3$ and at time $t = 0$ is placed at $x = -0.55$, with initial conditions ahead of the shock given by $\rho = 1.225(Kg/m^3)$, $p = 1.01325 \times 10^5(Pa)$ and zero velocity. Conditions behind are calculated from the Rankine-Hugoniot conditions.

The mesh consist on 256580 triangles. Boundary conditions are as follows: left boundary at $x = -0.65$ is defined as inflow condition with the corresponding state defined by the Rankine-Hugoniot conditions; at the right boundary at $x = 0.5$ we set an outflow condition. The remaining boundaries are solid reflecting boundaries.

For the results shown we used the third order ADER scheme along with the CT solver for the Derivative Riemann Problem and Courant number $C_{cfl} = 0.45$. Figures 12 to 15 display

Mesh	L_1 error	O_1	L_2 error	O_2	L_∞ error	O_∞
224	1.95×10^{00}		4.60×10^{-1}		3.71×10^{-1}	
898	3.86×10^{-1}	2.49	7.19×10^{-2}	2.85	6.99×10^{-2}	2.57
3618	2.90×10^{-2}	3.69	7.23×10^{-3}	3.27	8.40×10^{-3}	3.02
14402	1.31×10^{-3}	4.48	3.44×10^{-4}	4.40	2.12×10^{-4}	5.32
57694	1.48×10^{-5}	6.60	3.85×10^{-6}	6.62	2.54×10^{-6}	6.52

Table 8: Convergence rates test: fifth order method.

Schlieren images for the density at times $t = 7.93 \times 10^{-4}$, $t = 1.41 \times 10^{-3}$, $t = 1.85 \times 10^{-3}$ and $t = 2.20 \times 10^{-3}$ respectively. The shock wave propagates to the right, reflects from the solid triangle and generates a circular reflection shock. The two expansion waves created by the vertexes v_2 and v_3 produce regions of low density and pressure. See Fig. 16 for a three dimensional image of the density at time $t = 2.20 \times 10^{-3}$.

The main physical features of the flow look reasonable, as compared with analogous problems for which there are experimental results, see [21].

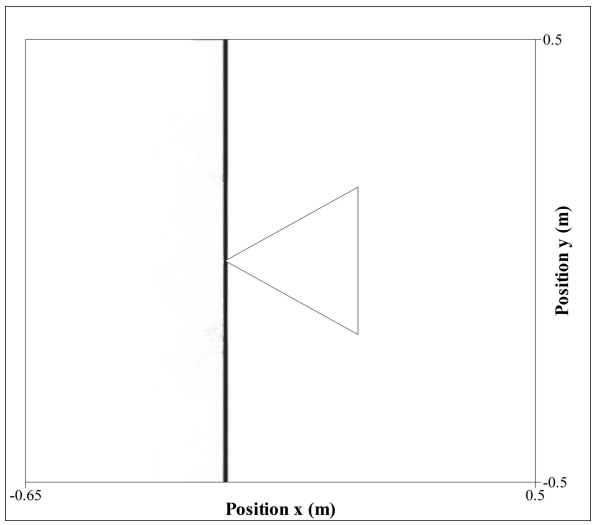

Figure 12: Shock wave reflection problem. Schlieren image for density at time $t = 7.93 \times 10^{-4}$. The shock wave begins the interaction with the triangle.

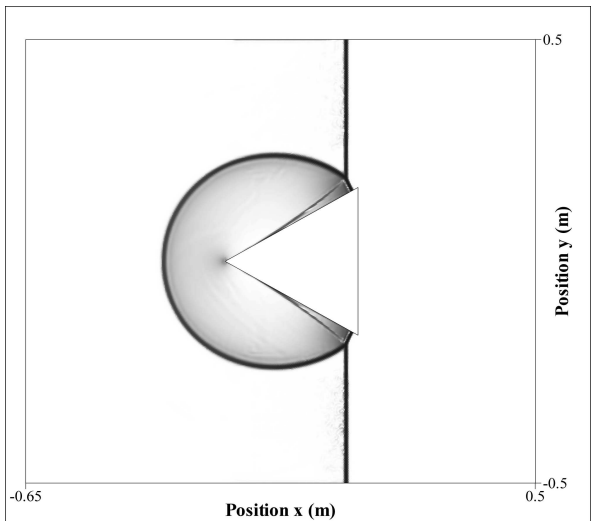

Figure 13: Shock wave reflection problem. Schlieren image for density at time $t = 1.41 \times 10^{-3}$. The shock wave reflects from the edges of the triangle and generates a single Mach reflection pattern.

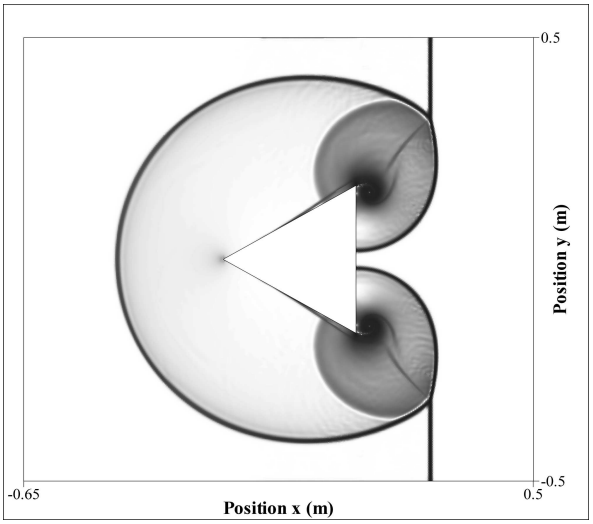

Figure 14: Shock wave reflection problem. Schlieren image for density at time $t = 1.85 \times 10^{-3}$. The shock wave generates two expansive waves over the corners of the triangle. A slip surface is produced from the interaction of the original shock wave and the reflected one.

7 Summary and concluding remarks

In this paper we have studied three methods for solving the Derivative Riemann Problem for non-linear systems of hyperbolic balance laws. The techniques have been illustrated for the compressible Euler equations of gas dynamics. One of the methods results from a re-interpretation of the scheme proposed by Harten et al. [10]. Another method results from a modification of the DRP solver of Titarev and Toro [35]. All three DRP solvers are assessed systematically on a range of *local* derivative Riemann problems. It is found that for linear problems all three solvers are algebraically equivalent, as they are for non-linear systems with smooth initial conditions throughout. For non-linear systems with discontinous initial conditions the solvers tend to differ amongst themselves, and from the reference solution, as the jump in the initial conditions at the origin increases. For small jumps all solvers tend to give an accurate solution for short times, as one would expect.

We have also implemented the DRP solvers, locally, in the context of high-order finite volume numerical methods of the ADER type, on unstructured meshes. Schemes of up to fifth order of accuracy in space and time for the two-dimensional compressible Euler equations have been constructed. The empirically obtained convergence rates correspond to the theoretically expected orders of accuracy. An illustration of the potential capabilities of our high order methods to solve realistic problems on complex domains, using unstructured meshes, has also been given.

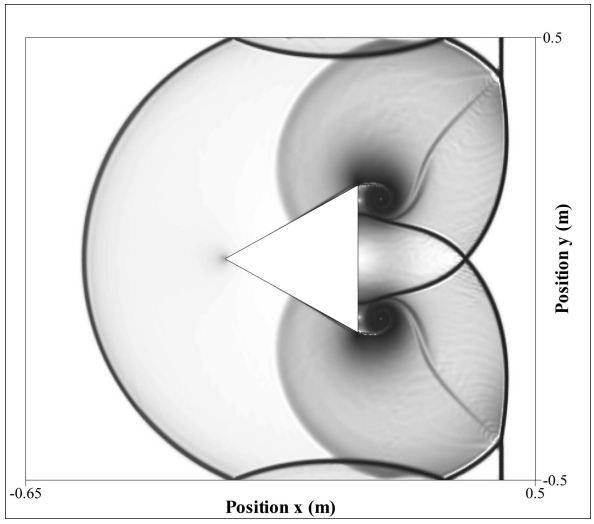

Figure 15: Shock wave reflection problem. Schlieren image for density at time $t = 2.20 \times 10^{-3}$. Two vortexes evolve behind the triangle. The expansion waves interact with the shock and with the boundaries.

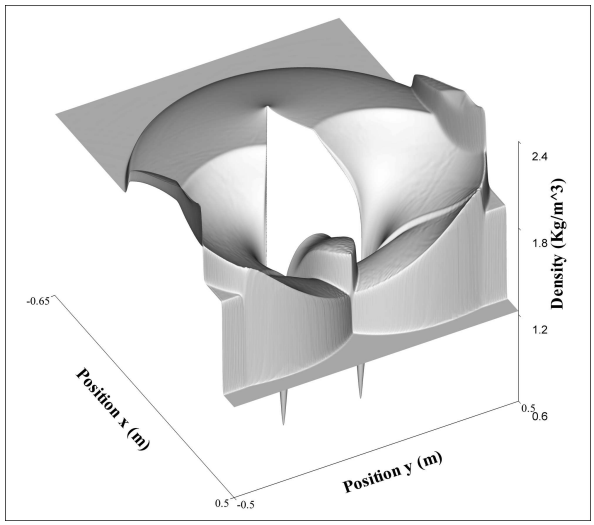

Figure 16: Shock wave reflection problem. Schlieren image for density at time $t = 2.20 \times 10^{-3}$. Three dimensional image for the density.

References

[1] M. Ben-Artzi and J. Falcovitz. A Second Order Godunov–Type Scheme for Compressible Fluid Dynamics. *J. Comput. Phys.*, 55:1–32, 1984.

[2] M. Ben-Artzi and J. Falcovitz. *Generalized Riemann Problems in Computational Fluid Dynamics*. Cambridge University Press, 2003.

[3] A. Bourgeade, P. LeFloch, and P. A. Raviart. An Asymptotic Expansion for the Solution of the Generalized Riemann Problem. Part 2: Application to the Euler Equations of Gas Dynamics. *Ann. Inst. Henri Poincaré. Analyse non Lineáre*, 6(6):437–480, 1989.

[4] P. Colella. A Direct Eulerian MUSCL Scheme for Gas Dynamics. *SIAM J. Sci. Stat. Comput.*, 6:104–117, 1985.

[5] M. Dumbser. *Arbitrary High Order Schemes for the Solution of Hyperbolic Conservation Laws in Complex Domains*. PhD thesis, Institut für Aero- un Gasdynamik, Universität Stuttgart, Germany, 2005.

[6] M. Dumbser and M. Käser. Arbitrary high order non-oscillatory finite volume schemes on unstructured meshes for linear hyperbolic systems. *J. Comp. Phys.(accepted)*, 00:000–000, 2006.

[7] M. Dumbser and C. D. Munz. ADER Discontinuous Galerkin Schemes for Aeroacoustics. *Comptes Rendus Mécanique*, –:to appear, 2005.

[8] J. Glimm. Solution in the Large for Nonlinear Hyperbolic Systems of Equations. *Comm. Pure. Appl. Math.*, 18:697–715, 1965.

[9] S. K. Godunov. Finite Difference Methods for the Computation of Discontinuous Solutions of the Equations of Fluid Dynamics. *Mat. Sb.*, 47:271–306, 1959.

[10] A. Harten, B. Engquist, S. Osher, and S. R. Chakravarthy. Uniformly High Order Accuracy Essentially Non–oscillatory Schemes III. *J. Comput. Phys.*, 71:231–303, 1987.

[11] A. Harten and S. Osher. Uniformly High–Order Accurate Nonoscillatory Schemes I. *SIAM J. Numer. Anal.*, 24(2):279–309, 1987.

[12] C. Hu and C. W. Shu. Weighted Essentially Non-oscillatory Schemes on Triangular Meshes. *J. Comp. Phys.*, 150:97–127, 1999.

[13] G. S. Jiang and C. W. Shu. Efficient Implementation of Weighted ENO Schemes. *J. Comp. Phys.*, 126(130):202–228, 1996.

[14] M. Käser. *Adaptive Methods for the Numerical Simulation of Transport Processes*. PhD thesis, Institute of Numerical Mathematics and Scientific Computing, University of Munich, Germany, 2003.

[15] M. Käser. ADER Schemes for the Solution of Conservation Laws on Adaptive Triangulations. Mathematical Methods and Modelling in Hydrocarbon Exploration and Production. Springer-Verlag (to appear), 2004.

[16] M. Käser and A. Iske. Adaptive ADER Schemes for the Solution of Scalar Non-Linear Hyperbolic Problems. *J. Comput. Phys.*, 205:486–508, 2005.

[17] P. Le Floch and P. A. Raviart. An Asymptotic Expansion for the Solution of the Generalized Riemann Problem. Part 1: General Theory. *Ann. Inst. Henri Poincaré. Analyse non Lineáre*, 5(2):179–207, 1988.

[18] P. Le Floch and L. Tatsien. A Global Asymptotic Expansion for the Solution of the Generalized Riemann Problem. *Ann. Inst. Henri Poincaré. Analyse non Lineáre*, 3:321–340, 1991.

[19] I. S. Men'shov. Increasing the Order of Approximation of Godunov's Scheme Using the Generalized Riemann Problem. *USSR Comput. Math. Phys.*, 30(5):54–65, 1990.

[20] Kolgan V. P. Application of the Principle of Minimum Derivatives to the Construction of Difference Schemes for Computing Discontinuous Solutions of Gas dynamics (in Russian). *Uch. Zap. TsaGI, Russia*, 3(6):68–77, 1972.

[21] H. Schardin. In Proc. VII Int. Cong. High Speed Photg. Darmstadt. O. Helwich Verlag, 1965.

[22] T. Schwartzkopff. *Finite–Volumen Verfahren hoher Ordnung und heterogene Gebietszerlegung ü die numerische Aeroakustik*. PhD thesis, Institut für Aero- un Gasdynamik, Universität Stuttgart, Germany, 2005.

[23] T. Schwartzkopff, Munz C.D, and E. F. Toro. ADER: High-Order Approach for Linear Hyperbolic Systems in 2D. *J. Scientific Computing*, 17:231–240, 2002.

[24] T. Schwartzkopff, M. Dumbser, and Munz C.D. Fast High-Order ADER Schemes or Linear Hyperbolic Equations. *J. Comput. Phys.*, 197:532–539, 2004.

[25] C. Shu and S. Osher. Efficient Implementation of Essentially Non–oscillatory Shock–Capturing Schemes II. *J. Comput. Phys.*, 83:32–78, 1988.

[26] C. W. Shu and S. Osher. Efficient Implementation of Essentially Non–oscillatory Shock–Capturing Schemes. *J. Comput. Phys.*, 77:439–471, 1988.

[27] Y. Takakura and E. F. Toro. Arbitrarily Accurate Non-Oscillatory Schemes for a Non-Linear Conservation Law. *J. Computational Fluid Dynamics*, 11(1):7–18, 2002.

[28] V. A. Titarev and E. F. Toro. ADER: Arbitrary High Order Godunov Approach. *J. Scientific Computing*, 17:609–618, 2002.

[29] V. A. Titarev and E. F. Toro. ADER Schemes for Three-Dimensional Hyperbolic Systems. *J. Comput. Phys.*, 204:715–736, 2005.

[30] E. F. Toro. *Riemann Solvers and Numerical Methods for Fluid Dynamics*. Springer–Verlag, 1997.

[31] E. F. Toro. Primitive, Conservative and Adaptive Schemes for Hyperbolic Conservation Laws. In *Numerical Methods for Wave Propagation. Toro, E. F. and Clarke, J. F. (Editors)*, pages 323–385. Kluwer Academic Publishers, 1998.

[32] E. F. Toro. *Riemann Solvers and Numerical Methods for Fluid Dynamics, Second Edition*. Springer–Verlag, 1999.

[33] E. F Toro and Titarev V. A. Derivative Riemann Solvers for Systems of Conservation Laws and ADER Methods. *J. Comput Phys.*, 212(1):150–165, 2006.

[34] E. F. Toro, R. C. Millington, and L. A. M. Nejad. Towards Very High–Order Godunov Schemes. In *Godunov Methods: Theory and Applications. Edited Review, E. F. Toro (Editor)*, pages 905–937. Kluwer Academic/Plenum Publishers, 2001.

[35] E. F. Toro and V. A. Titarev. Solution of the Generalised Riemann Problem for Advection-Reaction Equations. *Proc. Roy. Soc. London A*, 458:271–281, 2002.

[36] E. F. Toro and V. A. Titarev. ADER Schemes for Scalar Hyperbolic Conservation Laws with Source Terms in Three Space Dimensions. *J. Comput. Phys.*, 202(1):196–215, 2005.

[37] B. van Leer. Towards the Ultimate Conservative Difference Scheme I. The Quest for Monotonicity. *Lecture Notes in Physics*, 18:163–168, 1973.

[38] B. van Leer. Multidimensional Explicit Difference Schemes for Hyperbolic Conservation Laws. In *Computing Methods in Applied Sciences and Engineering*. Elsevier Science Publishers B.V., 1984.